Magnetization jumps and thermal cycling effect induced by impurities in $Pr_{0.6}Ca_{0.4}MnO_3$

2002 J. Phys.: Condens. Matter 14 11809

(http://iopscience.iop.org/0953-8984/14/45/322)

INSTITUTE OF PHYSICS PUBLISHING JOURNAL OF PHYSICS: CONDENSED MATTER

J. Phys.: Condens. Matter **14** (2002) 11809–11819 PII: S0953-8984(02)38242-0

Magnetization jumps and thermal cycling effect induced by impurities in $Pr_{0.6}Ca_{0.4}MnO_3$

A Maignan[1], **S Hébert, V Hardy, C Martin, M Hervieu and B Raveau**

Laboratoire CRISMAT, UMR CNRS ISMRA 6508, 6 bd Maréchal Juin, 14050 Caen Cedex, France

E-mail: antoine.maignan@ismra.fr

Received 17 June 2002, in final form 10 September 2002
Published 1 November 2002
Online at stacks.iop.org/JPhysCM/14/11809

Abstract

Staircase-like magnetic-field-driven magnetization curves ($M(H)$) from an antiferromagnetic to a ferromagnetic state have been obtained in $Pr_{0.6}Ca_{0.4}MnO_3$ substituted at the Mn site. Although both nonmagnetic (Ga^{3+}, $3d^{10}$) and magnetic (Cr^{3+}, $3d^3$) substituted cations are able to induce an insulator-to-metal transition, a very distinct magnetic behaviour is observed as the impurity content increases. In the case of Ga^{3+}, the induced ferromagnetic fraction goes through an optimum ($\sim$40%) for 3% Ga whereas, with only 2% of Cr^{3+}, this fraction reaches 95%. Interestingly, as the ferromagnetic fraction is not too high ($\leqslant$50%), staircase-like $M(H)$ curves are observed at low temperature. The number of magnetization jumps necessary to reach a complete ferromagnetic state is smaller than that of the Mn-site substituted $Pr_{0.5}Ca_{0.5}MnO_3$. Moreover, in the case of Ga^{3+}, there exists a clear relationship between the thermal cycling effect and the reproducibility of the M jumps. These results are discussed in the framework of a martensitic-like transition.

1. Introduction

Among the numerous interesting physical properties exhibited by the perovskite manganites, the cooperative orbital and/or charge ordering (OO/CO) phenomena are very fascinating [1]. In particular, the collapse of these ordered structures induced by external perturbations has dramatic consequences on transport properties since, for instance, the magnetic-field-driven insulator-to-metal (I–M) transition is responsible for the colossal magnetoresistance (CMR) of this class of transition metal oxides [2]. However, the stability of the Mn^{3+} and Mn^{4+} OO/CO checkerboard structure in the prototypical, half-doped manganites [3], $Ln_{0.5}Ca_{0.5}MnO_3$ (where Ln = lanthanide, except La), explains the high magnetic value required to melt the CE-type, antiferromagnetic (antiferromagnetically coupled Mn^{3+}–O–Mn^{4+} ferromagnetic zig-zag chains) OO/CO phase [4] into a ferromagnetic one i.e. 25 T for $Pr_{0.5}Ca_{0.5}MnO_3$ [5].

[1] Author to whom any correspondence should be addressed.

This critical magnetic field can be dramatically reduced by creating ferromagnetic regions in the antiferromagnetic matrix, the former acting as nucleation centres for the metamagnetic, AFM-to-FM transition [5]. From the chemical point of view, this phase separation [6–8] is promoted by disorder, either at the A-site of the perovskite, such as the size mismatch of the cations, or at the Mn-site by substitution of cations which hinders the OO/CO process to the benefit of the ferromagnetic metallic state [9–16]. Recently, we have found that the AFM-to-FM metamagnetic transitions in Mn-site-doped $Pr_{0.5}Ca_{0.5}MnO_3$ manganites exhibit several abrupt magnetization (M) jumps driven by an external magnetic field for low enough temperatures ($\leqslant$10 K) [17–19]. In particular, the largest M step values are reached for 3% of d^{10} cations (Ga^{3+}, Sn^{4+}, In^{3+}) substituted for Mn in $Pr_{0.5}Ca_{0.5}MnO_3$ [18]. The beneficial effect of d^{10} cations compared to d^0 cations or even magnetic cations (($Co^{2+}(3d^7)$ and $Ni^{2+}(3d^8)$)), also not understood, has shown that the electronic configuration of the impurity plays a role in the magnetic-field-driven magnetization process. To extend our work to $Pr_{1-x}Ca_xMnO_3$ compositions with $x \neq 0.5$, the $x < 0.5$ side is more appropriate since the critical field of the AFM-to-FM transition increases for $x > 0.5$, i.e. as the Mn^{4+} content increases the OO/CO structure becomes more difficult to destabilize by the impurity doped at the Mn site [20]. Thus, our study has been focused on $Pr_{0.6}Ca_{0.4}MnO_3$, which exhibits a canted CE-type AFM structure ($T_N \approx 170$ K) [21–23]. As a consequence, the background state of the $Pr_{0.6}Ca_{0.4}MnO_3$ manganite already exhibits a smaller critical field, $H_c \sim 8$ T [5, 24], than that of $Pr_{0.5}Ca_{0.5}MnO_3$, $H_c \sim 25$ T [5]. Moreover, as previously reported, the IM transition in zero magnetic field can be induced by doping at the Mn site in $Pr_{0.6}Ca_{0.4}MnO_3$with either magnetic or nonmagnetic cations [25] whereas such transitions are only induced by magnetic substituted cations in the case of $Pr_{0.5}Ca_{0.5}MnO_3$ [9–16].

In the following we report on abrupt magnetization jumps induced at 2.5 K by magnetic (Cr^{3+}, $3d^3$) and nonmagnetic (Ga^{3+}, $3d^{10}$) trivalent cations, in $Pr_{0.6}Ca_{0.4}MnO_3$. A clear difference in the transport properties is evidenced between the two series $Pr_{0.6}Ca_{0.4}Mn_{1-x}M_xO_3$, showing that the electronic configuration of the substituted cation and its substitution level play a dramatic role. Moreover, the role of the thermal cycling effect [26, 27] on the step feature in the $M(H)$ curves is studied.

2. Experimental details

All the $Pr_{0.6}Ca_{0.4}Mn_{1-x}M_xO_3$ ceramic samples with M = Ga^{3+} and Cr^{3+} have been prepared according to the process given in [25]. X-ray diffraction and electron microscopy (diffraction and coupled EDS) were used to confirm the purity of the samples and adequate agreement between the nominal and actual compositions. The electron diffraction (ED) study was carried out versus temperature with a JEOL 2010 electron microscope. The physical properties have been checked by means of ac magnetic susceptibility (χ', χ''), four-probe resistivity (ρ) and dc magnetization (M). As previously shown, the physical properties are history-dependent. In order to compare the properties probed by the different techniques (χ_{ac}, M, ρ), different pieces of virgin samples have been used. Prior to the magnetic-field-dependent M and ρ isothermal measurements, the samples were cooled with temperature sweep rates always in the range 5–10 K min^{-1}. For both types of measurements, the magnetic field was swept at 0.025 T s^{-1}. As shown later on, the content of doped cation is critical for the jump observation.

3. Results

For the $Pr_{0.5}Ca_{0.5}Mn_{0.95}M_{0.05}O_3$ case [16], the greater ability of the magnetic M cations to weaken the OO/CO CE-type structure was confirmed by the induced fractions of metallic FM

Table 1. Ferromagnetic fraction at 5 K, temperature of IM transition on the first cooling resistivity curve, resistivity value at 5 K (after the first cooling), critical field H_{S1} of the first magnetization jump on the virgin $M(H)$ curve registered at 2.5 K, and number of steps on the first $M(H)$ curve at 2.5 K. Note that, for the $x = 0.04$ Ga sample, ρ is too high to be measured in the vicinity of T_{IM} so that the T_{IM} value is a crude estimation.

x	Ferromagnetic fraction (%)	T_{IM} (K)	$\rho_{5\,K}$ (Ω cm)	H_{S1} (T) (2.5 K)	Step number at 2.5 K
$Pr_{0.6}Ca_{0.4}Mn_{1-x}Ga_xO_3$					
0.01	6	SC	$>10^6$	2.75	2
0.02	23	72	0.2	2.50	2
0.03	40	68	0.1	2.50	1
0.04	16	∼50	2	1.50	2
$Pr_{0.6}Ca_{0.4}Mn_{1-x}Cr_xO_3$					
0.005	9	62	2	2.75	2
0.01	51	120	0.009	2.75	1
0.02	95	140	0.002	No step	0

phase always beyond the percolation threshold, whereas these fractions reached a maximum of only 2% in the case of nonmagnetic cations. For the series $Pr_{0.6}Ca_{0.4}Mn_{1-x}M_xO_3$ under study, the FM fractions have been similarly deduced from the magnetization value measured under 0.25 T at 5 K (table 1). The contribution of the AFM parts has been removed by subtracting the magnetization of the pure CE-type AFM, $Pr_{0.5}Ca_{0.5}MnO_3$, measured in the same field value. Finally, the resulting magnetization value was divided by the value obtained in the same field for a reference sample, $Pr_{0.5}Ca_{0.5}Mn_{0.95}Ru_{0.05}O_3$, which is ∼100% ferromagnetic. As shown in table 1, the FM fractions obtained for the $Pr_{0.6}Ca_{0.4}Mn_{1-x}Cr_xO_3$ are much higher than those of the Ga series: for instance, these fraction values are 51 and 6% for 1% of Cr and Ga, respectively. These data show also that the FM fraction goes through a maximum value for $x = 0.03$ in the Ga series.

4. Thermal cycling effect: T-dependent resistivity

In a sample exhibiting an homogeneous chemical composition, the coexistence at low temperature of two kinds of phases with different cell parameters, one metallic FM and the other insulating AFM, is at the origin of the analogy with martensitic transitions [29]. The AFM phase exhibits a crystallographic structure close to that of the FM one but is more distorted due to the Mn^{3+}/Mn^{4+} OO/CO phenomenon [28]. This must induce strains in the interfacial regions. This competition between two different phases of close free energies makes the physics of the AFM ↔ FM transitions very comparable to the large family of martensitic-like transitions [19]. In this respect, the martensitic-like transformation from AFM-OO/CO to FM can be driven by either cooling (temperature scan) or increasing the external magnetic field at low temperature (field scan). Accordingly, one expects some equivalence between the effects of thermal and magnetic cycling. In the phase-separated manganites, the thermal cycling effect is observed simultaneously in resistivity and magnetization [26, 27]. As the samples undergo successive cooling–warming cycles, for instance from 300 K down to 5 K and then up to 300 K again, these phase-separated manganites show a progressive concomitant decrease and increase of the magnetization and the resistivity, respectively, with the increasing number of thermal cycles.

The successive $\rho(T)$ curves collected upon cooling in zero magnetic field from 300 down to 5 K for the series $Pr_{0.6}Ca_{0.4}Mn_{1-x}Cr_xO_3$ (figure 1) illustrate this effect. As soon as the content

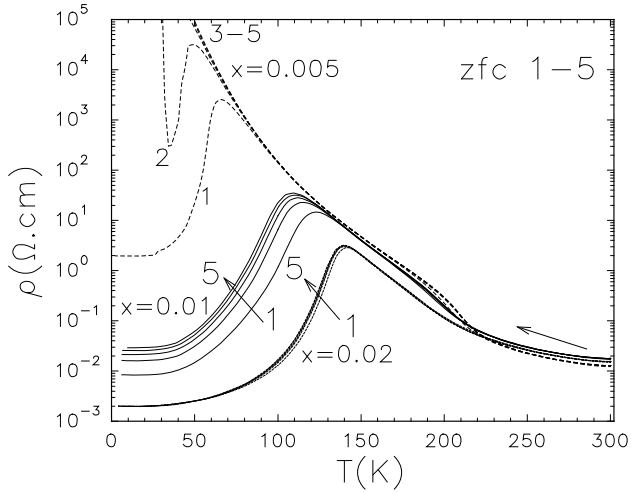

Figure 1. Successive zero-field resistivity curves (1–5) measured upon cooling from 300 down to 5 K (arrow) for $Pr_{0.6}Ca_{0.4}Mn_{1-x}Cr_xO_3$ ($x = 0.005$, 0.01 and 0.02).

of the substituted cation is large enough to induce a fraction of FM metallic phase beyond the percolation threshold (∼16%), an I–M transition is observed on the $\rho(T)$ curve whereas the pristine compound, $Pr_{0.6}Ca_{0.4}MnO_3$ remains insulating for the lowest T values [27]. In the Ga series, 1% substitution is not sufficient (FM fraction is only 6%) whereas for Ga-2% (FM fraction of 23%) an I–M transition occurs at 72 K (table 1). Note that the large unsettled background state of the 5% Cr-doped sample deduced from the comparison of the successive $\rho(T)$ curves in figure 1 makes the FM fraction determination very uncertain since, as shown later on, this fraction is history-dependent. Although this fraction (9%), determined in a virgin sample, lies below the percolation threshold, the first $\rho(T)$ curve exhibits an I–M transition at 62 K, but from the third temperature scan the I–M transition is suppressed. Nonetheless, as the Cr content is increased to 1%, the FM fraction jumps to 51% and the samples are almost fully ferromagnetic for 2% Cr (table 1). In contrast, in the Ga series the FM fraction goes through a maximum value (40% for $x = 0.03$) and then decreases for $x = 0.04$. Interestingly, for low contents of substitutions ($\leqslant$1 and 3% for Cr and Ga, respectively), the successive $\rho(T)$ curves exhibit large thermal cycling effects, as illustrated for Cr in figure 1. The resistivity below T_{IM} increases systematically with the increasing number of thermal cycles and this effect is accompanied by a progressive T_{IM} decrease. For $Pr_{0.6}Ca_{0.4}Mn_{0.995}Cr_{0.005}O_3$ (figure 1), this effect is dramatic: between the first and second cycles, T_{IM} decreases by more than 10 K whereas simultaneously the resistivity at 5 K evolves from 2 Ω cm to a value too high to be measured with our experimental set-up ($>10^6$ Ω cm). In contrast, for $x = 0.02$, the effect of thermal cycling on the $\rho(T)$ curves is suppressed, as shown in figure 1.

5. Magnetization jumps and thermal cycling effect

In order to reveal a relation between the effect of thermal cycling on the resistivity and the low-temperature, field-driven magnetization curves, successive $M(H)$ half-loops have been recorded and between successive series of measurements, a thermal cycling from 2.5 to 300 K and to 2.5 K again has been performed. After each field-increasing branch, the change associated with the AFM-to-FM transition is irreversible and it is thus necessary to warm

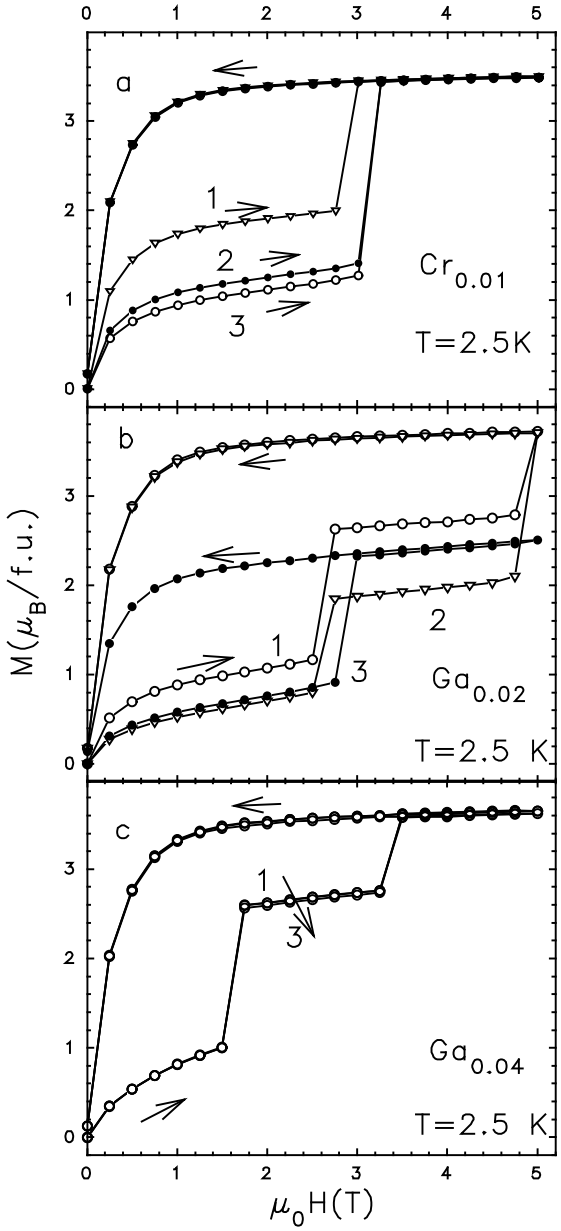

Figure 2. Successive isothermal ($T = 2.5$ K) $M(H)$ half-loops (1–3). Between successive measurements, the sample is warmed to 300 K and then cooled to 2.5 K in the absence of the magnetic field. (a) $Pr_{0.6}Ca_{0.4}Mn_{0.99}Cr_{0.01}O_3$, (b) $Pr_{0.6}Ca_{0.4}Mn_{0.98}Ga_{0.02}O_3$ and (c) $Pr_{0.6}Ca_{0.4}Mn_{0.96}Ga_{0.04}O_3$.

the sample (300 K within our process) in order to erase the field-induced modifications. In the Cr-substituted series, the $M(H)$ curves collected at 2.5 K are dependent on the thermal history for 0.5 and 1% as shown for the latter in figure 2(a). This is also the case for $x < 0.03$ in the series $Pr_{0.6}Ca_{0.4}Mn_{1-x}Ga_xO_3$ ($x = 0.02$ in figure 2(b)). For all these compositions where large

differences between successive $\rho(T)$ curves are observed, the thermal cycling induces a change in the $M(H)$ shape below the magnetic field value H_{S1} of the first magnetization jump. Below H_{S1}, as the cycle number increases the magnetization shifts down, which demonstrates that the FM fraction decreases. This indicates that the FM regions tend to disappear at the benefit of the OO/CO AFM ones, as if the thermal cycling was a 'training' effect for the stabilization of the AFM phases. Furthermore, the magnetic field of the first step H_{S1} exhibits a clear tendency to increase with the number of cycles (figures 2(a) and (b)) which is also consistent with the strengthening of the AFM state. These results are consistent with the ρ increase observed as the cycling number increases in figure 1. Clearly, the competition between the insulating OO/CO AFM and the metallic FM phases is history-dependent for the low-doping contents. But it becomes history-independent beyond a critical composition in the case of the Ga series ($x = 0.04$ in figure 2(c)). This change from history-dependent to history-independent starts for the compositions $x \geqslant 0.03$, i.e. close to or beyond the FM optimum (highest T_{IM}, largest FM fraction (table 1)). The successive staircase $M(H)$ curves can thus exhibit two different kinds of behaviour depending on the existence or not of a thermal cycling effect on the $\rho(T)$ curves.

6. Structural transitions: ac magnetic susceptibility and electron diffraction

The existence of those interrelated thermal cyclings has motivated a study by ac magnetic susceptibility (χ', χ'') as a function of temperature, for which the low ac magnetic field ($h_{ac} = 10$ Oe) is not supposed to affect the magnetic state of the samples. Since the OO/CO setting is connected with a distortion of the orthorhombic structure of the charge-delocalized phases (either paramagnetic or ferromagnetic), one expects hysteresis in the magnetic transitions. Virgin samples have been measured during cooling from 350 down to 5 K and then warming up to 350 K. Only one hysteretic temperature range is observed in the undoped $Pr_{0.6}Ca_{0.4}MnO_3$ sample (figure 3(c)) since the cooling and warming curves are separated between $T \sim 100$ K and 250 K. For this composition the OO/CO temperature (T_{CO}) corresponds to ∼230 K [5, 21], and thus it makes sense to relate this irreversible region to the progressive structural transition from a disordered state to an OO/CO state beyond and below T_{CO}, respectively. Note also in figure 3(c) that below ∼100 K a small FM component develops, without hysteresis, consistent with the canted CE-type AFM structure [21]. For all substituted compositions characterized by history-dependent $M(H)$ curves, the $\chi'(T)$ curves are characterized by two hysteretic regions (figure 3(a), 2% Ga). Compared to the pristine compound, a transition towards a FM state is induced, extending between 30 and 120 K (figure 3(a)). This second hysteretic transformation, coexisting with the first one starting below T_{CO}, could be a partial structural transition from the OO/CO phase to a less distorted FM phase. The existence of an irreversibility, illustrated by the temperature shift of the χ' maximum from 30 up to 50 K for the temperature decreasing and increasing branches, respectively, is most probably associated with the structural transition. Thus, as the substituted sample is cooled down from 350 K (figure 3(a)), it would undergo two structural transitions extending over large T regions: from the disordered paramagnetic state above $T_{CO} \sim 230$ K to OO/CO state paramagnetic state below T_{CO}. Then, there is a second bump at ∼150 K, reminiscent of the long-range AFM setting found by neutron powder diffraction in $Pr_{0.6}Ca_{0.4}MnO_3$ and, finally, a partial structural transition starting below 80 K from the OO/CO AFM state to the FM state occurs. The last transition is not achieved since the χ' max value at ∼30–50 K is much smaller in comparison to the χ' maximum value obtained for $Pr_{0.6}Ca_{0.4}Mn_{0.98}Cr_{0.02}O_3$ for which the FM fraction is about 95% (figure 3(d)). Nevertheless, for the Ga-substituted samples with larger contents of doping cation which show no history-dependent properties (4% of Ga, figure 3(b)), the $\chi'(T)$ curves (cooling and warming) exhibit only one low temperature

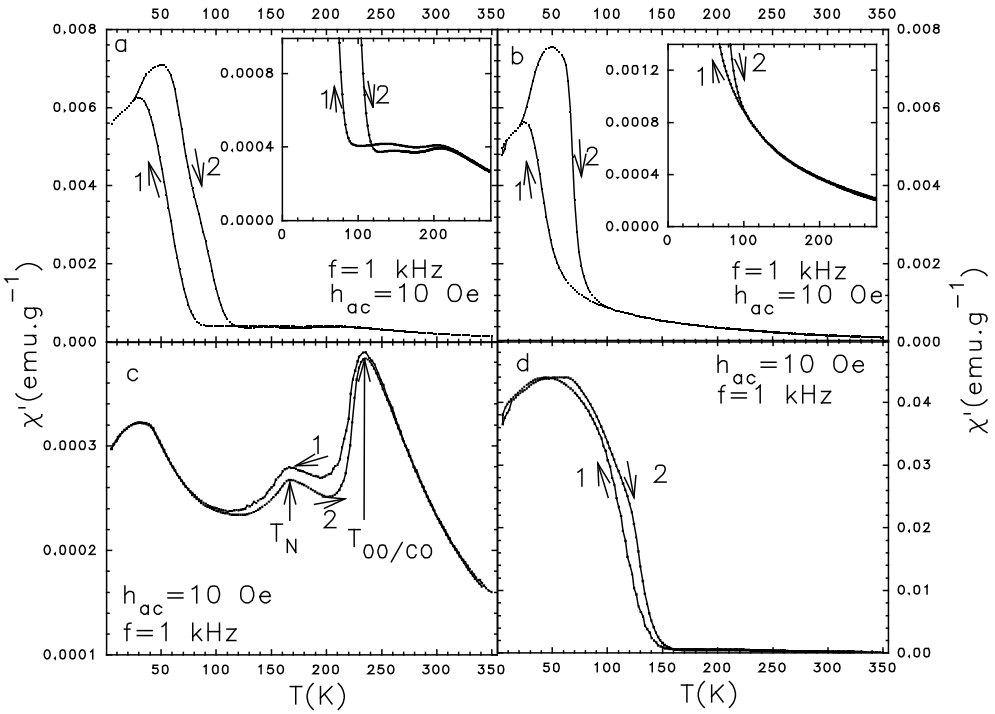

Figure 3. AC susceptibility (real part, χ') of (a) $Pr_{0.6}Ca_{0.4}Mn_{0.98}Ga_{0.02}O_3$ and (b) $Pr_{0.6}Ca_{0.4}Mn_{0.96}Ga_{0.04}O_3$. The $\chi'(T)$ curve for (c) $Pr_{0.6}Ca_{0.4}MnO_3$ and (d) $Pr_{0.6}Ca_{0.4}Mn_{0.98}Cr_{0.02}O_3$ are also shown. The samples are first cooled down to 5 K (arrow 1) and then warmed up to 350 K (arrow 2). Insets of (a) and (b) are enlargements of the $T_{OO/CO}$ regions.

hysteretic region. All the signatures of the OO/CO transition are suppressed on the $\chi'(T)$ curves (inset of figure 3(b)) so that the hysteresis, starting at ∼230 K for 2% of Ga, has disappeared, suggesting that the structural transition towards the OO/CO state is much less pronounced.

In order to probe the OO/CO microstructure by a more local technique, three samples were characterized by ED, at different temperatures between 92 K and RT. For each of the samples, numerous crystallites have been studied in order to collect statistically significant data. For the undoped compound $Pr_{0.6}Ca_{0.4}MnO_3$ at 92 K, a system of satellites is clearly observed, which involves a doubling of the *a* parameter. This superstructure is generated by the monoclinic distortion associated with the OO/CO phenomenon compared to the RT *Pnma* orthorhombic cell. The lattice images exhibit bright and less bright fringes, regularly spaced by 10.9 Å. The superstructure is stable under the electron beam. For the $Pr_{0.6}Ca_{0.4}Mn_{0.995}Cr_{0.005}O_3$ compound, the ED patterns and lattice images are very similar to those obtained for the undoped compound. A [010] pattern is given as an example in figure 4. The intense Bragg reflections of the perovskite cell are indexed in black; the extra satellites are indexed using the four *hklm* indices (in white) of a commensurate modulated superstructure ($\frac{1}{q}\vec{a}$ with $q = 0.5$). The lattice images also exhibit the regular system of fringes spaced 10.9 Å, which shows that the content of substituted element is not sufficient to generate discommensuration. In fact, the very important difference between the behaviours of $Pr_{0.6}Ca_{0.4}MnO_3$ and $Pr_{0.6}Ca_{0.4}Mn_{0.995}Cr_{0.005}O_3$ is the OO/CO instability of the latter under the electron beam. The satellites tend to disappear after too long an exposure (a few to a few tens of minutes) leading to a *Pnma*-type structure. In

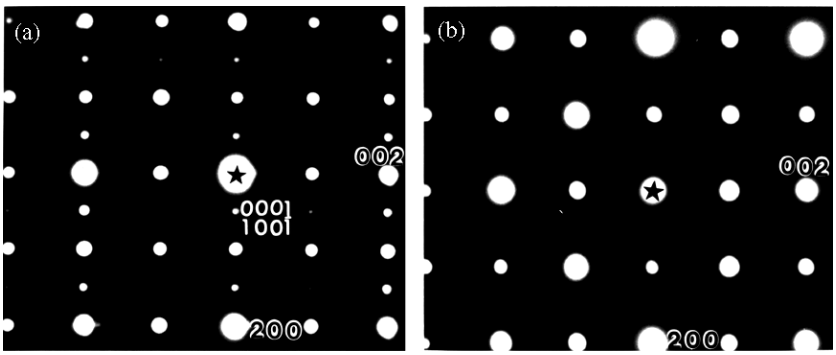

Figure 4. [010] ED pattern of $Pr_{0.6}Ca_{0.4}Mn_{0.995}Cr_{0.005}O_3$ collected at 92 K.

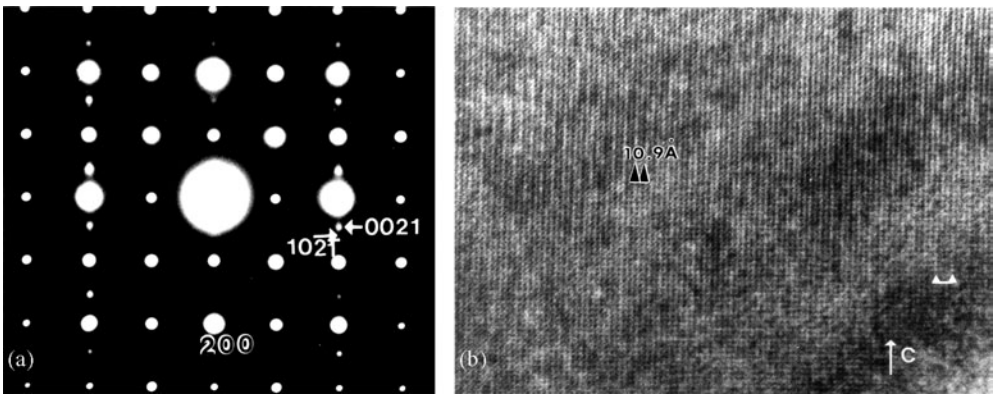

Figure 5. 92 K observations by electron microscopy for $Pr_{0.6}Ca_{0.4}Mn_{0.96}Ga_{0.04}O_3$: (a) [010] ED pattern; (b) corresponding lattice image showing the coexistence of locally modulated structures with a majority of non-modulated phase. The double black and white arrows are for the ∼10.9 and 16 Å modulations, respectively.

contrast, for the 4% Ga compound, the superstructure diffraction spots are not affected by the duration of the electron beam exposure. Although the OO/CO is thus more stable than for 0.5% Cr, the ED patterns recorded at 92 K show evidence of the incommensurate character of the modulated structure. The amplitude of the modulation is $q \sim 0.45$ (figure 5(a)). The lattice images show that the OO/CO phenomenon only occurs in the form of small domains, a few tens of nanometres wide, in a non-ordered matrix. This is illustrated in figure 5(b). In the larger part of the image, a two-dimensional system of perpendicular fringes, with a regular brightness and ∼5.45 Å spaced ($a_p\sqrt{2}$), is observed, in agreement with the *Pnma*-type contrast expected for a non-modulated structure. In the left part, bright and less bright fringes alternate, mainly 10.9 Å spaced, and locally ∼16 Å spaced (i.e. $3a_p\sqrt{2}$) in agreement with the modulation vector. Although performed at 92 K, this ED shows very distinct OO/CO features depending on the existence or not of thermal cycling effects. In particular, for the history-independent samples such as 4% Ga, the OO/CO is only set at short-range with an incommensurate superstructure which can be related to the absence of the OO/CO signature on the $\chi'(T)$ curves.

7. Discussion

The present study demonstrates that one or two abrupt jumps in the magnetization can be induced by substituting either magnetic or nonmagnetic cations for Mn in the canted CE-type AFM $Pr_{0.6}Ca_{0.4}MnO_3$. The observation of such features is thus not restricted to the doping at the Mn site in the half-doped manganites exhibiting a CE-type AFM structure such as $Pr_{0.5}Ca_{0.5}MnO_3$ but can be extended to the canted CE-type $Pr_{0.6}Ca_{0.4}MnO_3$ phase. It is also found that, similarly to the $Pr_{0.5}Ca_{0.5}MnO_3$ manganite, the substitutions by magnetic and nonmagnetic cations induce somewhat different behaviours. Unlike the series $Pr_{0.5}Ca_{0.5}Mn_{1-x}M_xO_3$, for which only magnetic M cations are able to induce a FM fraction beyond the percolation threshold, $Pr_{0.6}Ca_{0.4}Mn_{1-x}M_xO_3$ also exhibits an IM transition for M magnetic or nonmagnetic. However, the ability of the magnetic cation to induce this transition is much greater than that for the nonmagnetic one since the maximum FM fraction reaches 95% with only 2% of Cr, whereas an optimal FM fraction of 40% only is reached for 3% of Ga. This shows that a magnetic cation like Cr^{3+} is able to participate in the formation of an e_g band for the Mn^{3+}/Mn^{4+} cations by inducing a strong, double-exchange FM characterized by a larger T_C than the values obtained for nonmagnetic cations (table 1). Note that in the case of $Pr_{0.5}Ca_{0.5}MnO_3$, to reach a FM fraction close to ∼90%, it was necessary to substitute more Cr, 5% against only 2% in $Pr_{0.6}Ca_{0.4}MnO_3$ [16]. This also shows the weaker stability of the OO/CO structure in $Pr_{0.6}Ca_{0.4}MnO_3$, when compared to $Pr_{0.5}Ca_{0.5}MnO_3$, which is induced by the disorder created by the extra Mn^{3+} in comparison to the ideal $Mn^{3+}/Mn^{4+} = 1$ ratio. In this respect, the FM fraction induced by the Ga^{3+} substitution in $Pr_{0.6}Ca_{0.4}MnO_3$, culminating at ∼40% for $x = 0.03$, is much larger than for those measured in Ga-doped $Pr_{0.5}Ca_{0.5}MnO_3$ [16], reaching a maximum of only ∼2% for 5% Ga. This higher instability of the OO/CO structure in $Pr_{0.6}Ca_{0.4}MnO_3$ could explain why a maximum of two jumps in the $M(H)$ curves of these samples is sufficient to reach a completely saturated FM state within 5 T whereas three or four steps were observed for Ga-doped and Ni-doped $Pr_{0.5}Ca_{0.5}MnO_3$ manganites, respectively [17–19]. This is also consistent with the observation of only one magnetization jump when the FM is maximum in the Ga series.

It was proposed that the phase separation between the FM and OO/CO phases was responsible for strains at the interfaces between these regions and the temperature-dependent properties of the corresponding compounds were explained on the basis of a martensitic-like transformation [29, 30]. In the distorted OO/CO phase, the crystallographic unit cell is different to that of the FM phases which induces the strains [28]. This martensitic-like scenario has been further developed to explain the M jumps [19]. As the magnetic field increases, at low T, the nucleation of the OO/CO AFM-to-FM transformation starts around the regions surrounding the impurities. In the latter, the driving force acting on the spins can overcome the elastic constraints so that the interfaces between FM and OO/CO regions undergo a sudden motion. The local stress is thus released and, as an avalanche-like process, the FM regions grow, leading to a M jump. This avalanche process can be counterbalanced by the resulting increase of elastic energy compared to the decreasing magnetic energy. Consequently, the system can be frozen into another unstable state. Successive abrupt jumps between different unstable states, triggered by the magnetic field, could explain the existence of several steps on the $M(H)$ curve. Such martensitic transformations are sensitive to the defects, either pre-existing, such as impurities on the Mn sites, or induced by the thermal cycling.

By considering this scenario, the smaller number of steps on the $M(H)$ curves induced by the impurity in $Pr_{0.6}Ca_{0.4}MnO_3$ by comparison with $Pr_{0.5}Ca_{0.5}MnO_3$ is consistent with the fact that, at low temperature, the unit cell of $Pr_{0.6}Ca_{0.4}MnO_3$ is less distorted than that of $Pr_{0.5}Ca_{0.5}MnO_3$ [21]. From [21], it appears that the orthorhombic distortion, D, increases from

$\sim$0.5 to 1.2% for the $Pr_{0.6}Ca_{0.4}MnO_3$ and $Pr_{0.5}Ca_{0.5}MnO_3$ antiferromagnets, respectively. For the former, in the presence of the impurity, the strains in the interfaces between the distorted AFM regions and the less-distorted FM ones should thus be weakened, which, in turn, makes the AFM-to-FM transition easier with less likelihood of intermediate states. Furthermore, in this framework the differences between successive $M(H)$ curves and the 'training' effect, responsible for the changes in the temperature-dependent resistivity, could be accounted for by microstructural defects induced by thermal cycling in the martensitic transition region. Similarly, structural defects induced by thermal cycling of the manganites under study could act as obstacles for the field-driven transitions. This 'training' effect reinforces the stability of the distorted phase. This explains that, as the cycling number increases, the magnetization for low magnetic-field values decreases and that the critical field for the first step increases, as shown for $Pr_{0.6}Ca_{0.4}Mn_{0.98}Ga_{0.02}O_3$ in figure 2(b).

One interesting feature exhibited by the series $Pr_{0.6}Ca_{0.4}Mn_{1-x}Ga_xO_3$ is the existence of the superposed $M(H)$ curves and an absence of a thermal cycling effect on the $\rho(T)$ curves for $x > 0.03$ (figure 2(c)) that was not observed in the Ga-doped $Pr_{0.5}Ca_{0.5}MnO_3$ series [17]. It should be recalled that this absence of a training effect is consistent with the absence of hysteresis at T_{CO} on the $\chi'(T)$ curves related to only short-range setting of the incommensurate OO/CO structure in the non-modulated matrix. This strongly suggests that the structural distortion starting below T_{CO} has been dramatically hindered by the impurity (the χ' drop at T_{CO} and T_N are no longer distinguishable on the curves). As a consequence, the setting of the AFM distorted phase is limited only to a short-range process. This would explain the absence of characteristic bumps at T_{CO} and of χ' hysteresis in this temperature range. Furthermore, for compositions with no training effect, i.e. beyond the optimum of the FM phase, the development of the FM state is also hindered by dilution by the nonmagnetic impurity on the Mn site. The background state of the sample at low temperature is thus a mixture of weakened short-range AFM and FM regions. This would explain why, despite the decrease of the strains at the interfaces, the steps in magnetization are still observed.

This becomes more understandable as one compares the differences in the properties induced by magnetic and nonmagnetic cations. If one considers that ferromagnetic clusters develop around the impurity and that 1% of Ga and Cr induce FM fractions of 6 and 51%, respectively, it becomes obvious that the size of the FM cluster is much larger for the Cr-doped sample, from which it turns out that the number of Mn participating in these clusters would be $\sim$5 and $\sim$50 for Ga and Cr, respectively. This illustrates the superiority of magnetic cations which reverse the surrounding spins by a 'domino effect' [12], as if the nonmagnetic cations were only involving their nearest Mn neighbours. This explains why the Cr substitution will rapidly make the $Pr_{0.6}Ca_{0.4}MnO_3$ sample almost 100% FM. This could also provide an intrinsic limit of the FM fraction to $\sim$50% in the case of nonmagnetic cations. For the latter, as the FM fraction becomes close to 50%, the additional substituted cations can be substituted equivalently in the FM and AFM regions. But in the case of the substitution in the FM regions, the extra Ga^{3+} will not contribute to the FM but, on the contrary, will tend to weaken it. This most probably explains the existence of an optimum in the FM fraction for the substitution by the nonmagnetic cation. This also suggests that the absence of the thermal cycling effect observed only close to or beyond the optimal concentration of nonmagnetic impurity is linked to the dilution of the FM regions by the impurity. This effect could create a change in the topology of the FM regions by directly breaking some of the FM Mn–O–Mn pathways. Accordingly, the interfaces at the boundaries between the AFM and FM regions will be strongly modified.

In summary, from this study and its comparison with previous ones [17–19], we believe that the staircase-like behaviour and the thermal cycling effects observed at low temperature in Mn-site-doped manganites are due to a martensitic-like mechanism. The nature of the dopant and

its concentration govern the induced FM fractions competing with the AFM ones. It is worth emphasizing that the AFM structure derived from the CE-type matrix also plays an important role. In these AFMs, nonmagnetic cations create only small FM clusters in comparison to magnetic cations such as chromium. For the former, as the FM fraction becomes close to 50%, the dilution of the FM regions by the additional nonmagnetic impurity is responsible for the existence of an optimum. This is supposed to modify strongly the topology of the FM regions, which in turn affects the martensitic-like transition.

References

[1] For a review, see
Rao C N R and Raveau B (ed) 1998 *Colossal Magnetoresistance, Charge Ordering and Related Properties of Manganese Oxides* (Singapore: World Scientific)
Tokura Y (ed) 1999 *Colossal Magnetoresistance Oxides* (London: Gordon and Breach)
[2] Kim K H, Uehara M, Hess C, Sarma P A and Cheong S W 2000 *Phys. Rev. Lett.* **84** 2961
[3] Goodenough J B 1955 *Phys. Rev.* **100** 564
[4] Wollan E O and Koehler W C 1955 *Phys. Rev.* **100** 545
[5] Tokunaga M, Miura N, Tomioka Y and Tokura Y 1998 *Phys. Rev.* B **57** 5259
[6] Mori S, Chen C H and Cheong S-W 1998 *Phys. Rev. Lett.* **81** 3972
[7] Moreo A, Yunoki S and Dagotto E 1999 *Science* **283** 2034
[8] Uehara M, Mori S, Chen C H and Cheong S-W 1999 *Nature* **399** 560
[9] Raveau B, Maignan A and Martin C 1997 *J. Solid State Chem.* **130** 162
Damay F, Martin C, Hervieu M, Raveau B, André G and Bourée F 1998 *Appl. Phys. Lett.* **73** 3772
[10] Maignan A, Damay F, Martin C and Raveau B 1997 *Mater. Res. Bull.* **32** 695
[11] Vanitha P V, Arulraj A, Raju A R and Rao C N R 1999 *C. R. Acad. Sci., Paris* **2** 595
[12] Martin C, Maignan A, Hervieu M, Autret C, Raveau B and Khomskii D I 2001 *Phys. Rev.* B **63** 174402
[13] Katsufuji T, Cheong S-W, Mori S and Chen C H 1999 *J. Phys. Soc. Japan* **68** 1090
[14] Hébert S, Maignan A, Frésard R, Hervieu M, Retoux R, Martin C and Raveau B 2001 *Eur. Phys. J.* B **24** 85
[15] Kimura T, Tomioka Y, Kumai R, Okinoto Y and Tokura Y 1999 *Phys. Rev. Lett.* **83** 3940
[16] Hébert S, Maignan A, Martin C and Raveau B 2002 *Solid State Commun.* **121** 229
[17] Hébert S, Hardy V, Maignan A, Mahendiran R, Hervieu M, Martin C and Raveau B 2002 *J. Solid State Chem.* **165** 6
[18] Hébert S, Maignan A, Hardy V, Martin C, Hervieu M and Raveau B 2002 *Solid State Commun.* **122** 335
[19] Hébert S, Maignan A, Hardy V, Martin C, Hervieu M, Raveau B, Mahendiran R and Schiffer P 2002 *Eur. Phys. J.* B **29** 419
[20] Tokunaga M, Miura N, Tomioka Y and Tokura Y 1998 *Phys. Rev.* B **57** 5259
[21] Jirák Z, Krupička S, Simša Z, Dlouhá M and Vratislav S 1985 *J. Magn. Magn. Mater.* **53** 153
[22] Frontera C, García-Muñoz J L, Llobet A, Respaud M, Broto J M, Lord J S and Planes A 2000 *Phys. Rev.* B **62** 3381
[23] Lees M R, Barrat J, Balakrishann G, McK Paul D and Ritter C 1998 *Phys. Rev.* B **58** 8694
[24] Tomioka Y, Asamitsu A, Kuwahara H, Moritono Y and Tokura Y 1996 *Phys. Rev.* B **53** R1689
[25] Damay F, Martin C, Maignan A and Raveau B 1997 *J. Appl. Phys.* **82** 6181
[26] Mahendiran R, Maignan A, Hervieu M, Martin C and Raveau B 2001 *J. Solid State Chem.* **160** 1
[27] Mahendiran R, Raveau B, Hervieu M, Michel C and Maignan A 2001 *Phys. Rev.* B **64** 064424
[28] Martin C, Maignan A, Damay F, Hervieu M, Raveau B, Jirak Z, André G and Bourée F 1999 *J. Magn. Magn. Mater.* **202** 11
[29] Uehara M and Cheong S-W 2000 *Europhys. Lett.* **52** 674
[30] Podzorov V, Kim B G, Kiryukhin V, Gershenson M E and Cheong S W 1994 *Phys. Rev. Lett.* **72** 1694